DOI: 10.1021/cg100488t

CRYSTAL GROWTH & DESIGN Article
2010, Vol. 10
3596–3607

Kinetic Theory of Crystallization of Nanoparticles

Katsuhiro Tsukimura,*[,†] Masaya Suzuki,[†] Yohey Suzuki,[†] and Takashi Murakami[‡]

[†]*Geological Survey of Japan, National Institute of Advanced Industrial Science and Technology, Tsukuba, Ibaraki 305-8567, Japan, and* [‡]*Department of Earth & Planetary Sciences, the University of Tokyo, Bunkyo, Tokyo 113-0033, Japan*

Received April 13, 2010; Revised Manuscript Received May 31, 2010

ABSTRACT: This paper describes a kinetic theory of the crystallization of nanoparticles, where nanoparticles are dissolving and crystals are forming in solution. The theory assumes that a crystal nucleates only on a nanoparticle, the crystal stops growing at a certain size, and the concentration of metal ion in solution is close to the solubility of the nanoparticles. On the basis of these assumptions, we have derived integral equations for $R(t)$ (crystal ratio as a function of time). We have solved the integral equations with a successive approximation method. When time t is less than t_{inflec} ($= r_{\max}/G$, $r_{\max}$ = maximum radius of crystal, G = growth rate of crystal), $R(t)$ is close to the 4th power of time; when t is larger than t_{inflec}, $R(t)$ is close to an exponential-type function. The kinetic theory has been applied successfully to the transformation of ferrihydrite nanoparticles to goethite or hematite crystals and the crystallization of TiO_2 and ZrO_2. The theory shows that the nucleation rate of the crystal essentially determines the crystallization rate and that an induction period is observed when the growth of the crystal is slow.

Introduction

The crystallization of colloidal nanoparticles (amorphous or poorly crystallized materials) in solution has been studied in many important systems. In particular, the transformation of ferrihydrite ($5Fe_2O_3 \cdot 9H_2O$) nanoparticles to goethite (FeOOH) or hematite (Fe_2O_3) crystals has been investigated at various temperatures and pHs.[1−7] This is because ferrihydrite nanoparticles are environmentally important: these nanoparticles are commonly observed in hot springs, mine drainages, and soils and adsorb many kinds of toxic elements such as Zn, Cu, As, U, and Pu.[8−12] The transformation of silica nanoparticles to quartz is also important for understanding the genesis of silica deposits.[13] The transformation of silica nanoparticles to silicalite crystals[14−17] and the crystallizations of TiO_2[18,19] and ZrO_2[20] nanoparticles have been studied because these crystals have useful properties and are synthesized from nanoparticles. Silicalite is used for the storage and separation of CO_2 and CH_4,[21] TiO_2 crystal has a photocatalytic property,[22] and ZrO_2 fine crystal is used for the raw materials for partially stabilized zirconia.[23]

Crystallization curves showing the crystal ratio as a function of time have been measured for the transformation of ferrihydrite to goethite or hematite,[1−5,7] silica nanoparticles to quartz,[8] TiO_2 nanoparticles to TiO_2 crystals,[19] and ZrO_2 nanoparticles to ZrO_2 crystals.[20] These crystallization curves have similar shapes. First, the concentrations of nanoparticles decrease exponentially. In particular, the transformation curve of ferrihydrite by Schwertmann et al.[2] is very close to an exponential curve. Second, induction periods are observed in some of the crystallization curves for ferrihydrite,[5,7] TiO_2,[19] and ZrO_2[20] nanoparticles.

Kinetic theories or models based on nucleation and growth mechanisms were applied to the crystallization of nanoparticles. Calculated values based on Avrami theory[24−26] fit fairly well with some experimental data of the crystallization of nanoparticles in solution. The Avrami theory has been, however, proposed for the crystallization of condensed matter such as glass, amorphous alloy, and melt but not for the crystallization of nanoparticles in solution. Therefore, even if the crystallization curve of Avrami theory fits with experimental data of nanoparticle crystallization in solution, its parameters have no physical meaning. Zhang et al. have proposed a kinetic theory for crystallization of nanoparticles in dry conditions, which successfully explains the crystallization rate of TiO_2 nanoparticles.[27] This theory assumes that a crystal stops growing at a certain size and that the growth rate is infinite. As a result, a crystal reaches a maximum size just after the crystal nucleates. Although this assumption can be applied to some cases, the assumption oversimplifies the condition when the growth of the crystal is slow.

This paper describes a new theory on the crystallization rate of nanoparticles in solution. The theory is based on a nucleation and growth mechanism and assumes that both nucleation and growth rates are finite and a crystal stops growing at a certain size. On the basis of these assumptions, we have derived integral equations for the crystal ratio. Solving the integral equations, we have calculated the crystal ratio as a function of time. Our theory shows how the rates of nucleation and crystal growth contribute to the crystallization rate and well explains previous experimental data on the crystallization rates of nanoparticles including the exponential decrease of nanoparticles and the presence of an induction period. The theory also shows the methods to control the crystallization rate and the size of crystals.

Theoretical Section

The theory considers the crystallization rate of nanoparticles in solution. For simplicity, we derive equations in a M−O−H system, where M denotes a metal element. In this system, nanoparticles ($MO_e(OH)_d$) are floating and dissolving in the solution, and crystals ($MO_e(OH)_f$) are forming in the solution. We assume that a crystal nucleates only on a nanoparticle (first assumption) and that the crystal stops growing at a certain size (second assumption). We also assume that X_{sol} (concentration of metal in solution) is close to $X_{\mathrm{nano\text{-}eq}}$ (solubility of nanoparticle) (third assumption). On the basis of these assumptions, we have derived integral equations for R (crystal ratio, that is, ratio of metal in the crystal to metal in the whole system). Solving the integral equations, we show how R

*E-mail: tsukimura-katsuhiro@aist.go.jp.

 Published on Web 06/30/2010

Table 1. List of Symbols[a]

symbol	unit	definition
b		t/t_{inflec}
β		τ/t_{inflec}
D_{close}		$\lvert J_{\mathrm{format}}-J_{\mathrm{nano\text{-}dissol}}\rvert/J_{\mathrm{nano\text{-}dissol}}$
G	m s^{-1}	radial growth rate of crystal (dr/dt)
I	s^{-1}	coefficient of nucleation rate (nucleation rate per nanoparticle)
J_{disssol}	mol s^{-1} L^{-1}	dissolution rate of crystals
J_{format}	mol s^{-1} L^{-1}	formation rate of crystals
$J_{\mathrm{nano\text{-}dissol}}$	mol s^{-1} L^{-1}	dissolution rate of nanoparticles
k	m^{-2} s^{-1}	coefficient of dissolution (or formation) rate of crystals
k_{nano}	m^{-2} s^{-1}	coefficient of dissolution (or formation) rate of nanoparticles
m	mol	amount of metal ion in one crystal with a maximum size
m_{nano}	mol	amount of metal ion in one nanoparticle
M	mol L^{-1}	moles of metal ion in all crystals in 1 L of solution
M_{nano}	mol L^{-1}	moles of metal ion in all nanoparticles in 1 L of solution
N	L^{-1}	number of crystals in 1 L of solution
N_{dead}	L^{-1}	number of crystals that finish growing in 1 L of solution
N_{nano}	L^{-1}	number of nanoparticles in 1 L of solution
p		$(I/G)(m/m_{\mathrm{nano}})r_{\mathrm{max}}$, parameter that determines the shape of R
r	m	radius of a crystal
r_{max}	m	radius of a crystal with maximum size
r_{nano}	m	radius of a nanoparticle
R		crystal ratio (ratio of metal ion in crystals to metal ion in the whole system)
R_0		Initial approximate equation of R
R_1		first approximate equation of R
R_2		second approximate equation of R
R_{nano}		nanoparticle ratio (ratio of metal ion in nanoparticles to metal ion in the whole system)
S	m^2 L^{-1}	surface area of crystals that are growing in 1 L of solution
S_{dead}	m^2 L^{-1}	surface area of crystals that finish growing in 1 L of solution
S_{nano}	m^2 L^{-1}	surface area of nanoparticles in 1 L of solution
t	s	time
τ	s	time at the nucleation of a crystal
t_{induc}	s	induction period
t_{inflec}	s	time at the inflection point
v	m^3 mol^{-1}	molar volume of metal ion in crystals
v_{max}	m^3	volume of a crystal with maximum size
v_{nano}	m^3 mol^{-1}	molar volume of metal ion in nanoparticles
V	m^3 L^{-1}	total volume of crystals in 1 L of solution
X_{eq}	mol L^{-1}	solubility of crystal in terms of metal concentration
$X_{\mathrm{nano\text{-}eq}}$	mol L^{-1}	solubility of nanoparticle in terms of metal concentration
X_{sol}	mol L^{-1}	concentration of metal ion in solution
X	mol L^{-1}	concentration of metal ion in crystals
X_{nano}	mol L^{-1}	concentration of metal ion in nanoparticles
X_{steady}	mol L^{-1}	concentration of metal ion in solution in a steady state

[a] Symbols used in the main text and in appendices.

changes with time. Table 1 lists symbols and their definitions used in the main text and the appendices.

Integral equations for *R*. Generally, the formation rate of crystal is proportional to the surface area of the crystal and the degree of supersaturation.[28] We can approximate that the degree of supersaturation is constant because we have assumed that X_{sol} is always close to $X_{\mathrm{nano\text{-}eq}}$ (third assumption). Then, the formation rate of the crystal is proportional only to the surface area of the crystal. The surface area of the crystal can be calculated from the nucleation and growth rates of the crystal.

On the basis of the above considerations, we here derive the integral equations that show how R increases with time. We assume that the crystals are spherical for simplicity. The radial growth rate of crystal, $G = dr/dt$, has a nonzero constant value as long as r is less than r_{max}, and the value becomes zero when $r = r_{\mathrm{max}}$. Because X_{sol} is always close to $X_{\mathrm{nano\text{-}eq}}$, I (the coefficient of nucleation rate) can be approximated to be constant and independent of time. The nucleation rate is given by IN_{nano} because the nucleation rate is proportional to N_{nano} (the number of nanoparticles) (first assumption). A crystal nucleating at time τ stops growing at time $\tau + t_{\mathrm{inflec}}$ ($t_{\mathrm{inflec}} = r_{\mathrm{max}}/G$). Then, at a later time t ($t = 0$ when the first crystal nucleates), a crystal that nucleates at time τ has a volume $4\pi/3\{(t-\tau)G\}^3$ when $t-\tau \le t_{\mathrm{inflec}}$ and a volume $4\pi/3(r_{\mathrm{max}})^3$ when $t-\tau \ge t_{\mathrm{inflec}}$. As shown later, R has an inflection point when $t = t_{\mathrm{inflec}}$. The number of crystals nucleated between time τ and $\tau + d\tau$ is given by $IN_{\mathrm{nano}}(\tau)\,d\tau$. As a result, the total volume of crystals that nucleated between time τ and $\tau + d\tau$ is given by

$$\begin{aligned} dV &= \frac{4\pi}{3}\{(t-\tau)G\}^3 IN_{\mathrm{nano}}(\tau)\,d\tau \quad (t-\tau \le t_{\mathrm{inflec}}) \\ dV &= \frac{4\pi}{3}(r_{\mathrm{max}})^3 IN_{\mathrm{nano}}(\tau)\,d\tau \quad (t-\tau \ge t_{\mathrm{inflec}}) \end{aligned} \tag{1}$$

Although we assumed that crystals are spherical for simplicity, our theory can treat crystals not only with spherical morphology but also with other morphologies. For example, the volume of a rectangular prism with growth rates of G_x, G_y, and G_z for the directions of x, y, and z, respectively, can be also expressed with eqs 1 by setting $G = (6G_xG_yG_z/\pi)^{1/3}$. By integrating eqs 1 and converting the volume of crystals to R (see Appendix A), we obtain equations

$$\begin{aligned} R(t_{\mathrm{inflec}}b) &= p\int_0^b (b-\beta)^3\{1-R(t_{\mathrm{inflec}}\beta)\}\,d\beta \quad (0 \le b \le 1) \\ R(t_{\mathrm{inflec}}b) &= p\Big[\int_0^{b-1}\{1-R(t_{\mathrm{inflec}}\beta)\}\,d\beta \\ &\quad + \int_{b-1}^b (b-\beta)^3\{1-R(t_{\mathrm{inflec}}\beta)\}\,d\beta\Big] \quad (1 \le b) \end{aligned} \tag{2}$$

where $b = t/t_{\mathrm{inflec}}$ and $\beta = \tau/t_{\mathrm{inflec}}$. We assume here that X_{sol} (concentration of metal ion in solution) is negligible compared with the amounts of M ions in nanoparticles and crystals, then we can approximate that $R + R_{\mathrm{nano}} = 1$. Parameter p is given by

$$p = I(r_{\mathrm{max}}/G)(m/m_{\mathrm{nano}}) \tag{3}$$

where m is the moles of metal ion in one crystal with a maximum size and m_{nano} is the moles of metal ion in one nanoparticle.

Solution When p Is Close to Zero. This is the case when no induction period is observed. Because $p \cong 0, 0 \le b - \beta \le 1$ and $0 \le 1 - R \le 1$, integrals in eqs 2 whose intervals are one or less than one are negligible. Therefore, eqs 2 are approximated by

$$\begin{aligned} R(t_{inflec}b) &= 0 && (0 \le b \le 1) \\ R(t_{inflec}b) &= p\int_0^{b-1} \{1 - R(t_{inflec}\beta)\}\, d\beta && (1 \le b) \\ &\cong p\int_0^{b} \{1 - R(t_{inflec}\beta)\}\, d\beta \end{aligned} \quad (4)$$

Combining eqs 4, we obtain an integral equation when p is close to zero:

$$R(t_{inflec}b) = p\int_0^{b} \{1 - R(t_{inflec}\beta)\}\, d\beta \qquad (0 \le b) \quad (5)$$

Differentiating of eq 5 gives a differential equation:

$$\frac{dR(t_{inflec}b)}{db} = p\{1 - R(t_{inflec}b)\} \quad (6)$$

Solving eq 6, we obtain the equation for crystal ratio as a function of time:

$$R(t) = 1 - \exp(-pt/t_{inflec}) \quad (7)$$

The value of p/t_{inflec} can be determined from the gradient of $\ln(1 - R(t))$ because $\ln(1 - R(t)) = -(p/t_{inflec})t$. Once we obtain the value of p/t_{inflec}, we can calculate the values of R using eq 7.

Solution When p Is Not Close to Zero. This is the case when an induction period is observed. The approximate equations of R for small b values are derived with a successive approximation method using eqs 2, and the values of R for large b are approximated with an exponential-type function. The successive approximation method starts with an initial approximate equation ($R_0 = 0$). We set $R_0 = 0$ because R is zero when $b = 0$ and close to zero when b is close to zero. Substituting R_0 into R in the right sides of eqs 2, we obtain first approximate equations:

$$\begin{aligned} R_1 &= pb^4/4 = p(t/t_{inflec})^4/4 && (0 \le b \le 1) \\ R_1 &= p(b - 0.75) = p(t/t_{inflec} - 0.75) && (1 \le b \le 1.75) \end{aligned} \quad (8)$$

We set the range of b less than 1.75 because the error of R becomes large when b is larger than 1.75. For b values larger than 1.75, we approximate R with an exponential-type function:

$$\begin{aligned} R_1 &= 1 - A\exp\{-B(b - 1.75)\} \\ &= 1 - A\exp\{-B(t/t_{inflec} - 1.75)\} \qquad (1.75 \le b) \end{aligned} \quad (9)$$

The parameters A and B are determined so as to connect smoothly with eqs 8 at 1.75 of b. As a result, we have obtained the values of the parameters as follows:

$$\begin{aligned} A &= 1 - p \\ B &= p/(1 - p) \end{aligned} \quad (10)$$

We can estimate the values of t_{inflec} and p by fitting a straight line with experimental data points having b values between 1.00 and 1.75. The straight line corresponds to the second equation of eqs 8. Time at the intersection of the straight line with the vertical axis ($R = 0$) gives a value of t_{induc} (Figure 2). The second equation of eqs 8 shows that $t_{inflec} = {}^4/_3 t_{induc}$, which enables us to calculate the value of t_{inflec}. The gradient of the straight line gives a value of p/t_{inflec} from which we can calculate the value of p.

Once we obtain the values of t_{inflec} and p, we can calculate the values of R using eqs 8 and 9. Figure 1 shows the errors for the first and second approximate equations. Because the errors of the first approximate equations are < 0.025 when $p < 0.5$ (Figure 1a), the first approximate equations are accurate enough for R calculations for $p < 0.5$. However, when $p > 0.5$, the errors can be larger than 0.025. Therefore, the second approximate equations (Appendix B) should be used for $p > 0.5$; the errors of the second approximate equations are < 0.02 in all ranges of p and R (Figure 1b). When we need extremely accurate calculated values of R, we can use a numerical calculation method (Appendix C).

Physical Meanings of R. Figure 2 shows a general trend of R variation as a function of time, and Figure 3 schematically shows how nucleation and growth rates affect R variation. When the reaction starts ($t = 0$), the first crystal nucleates in solution. As time proceeds, many crystals nucleate on nanoparticles and grow. When

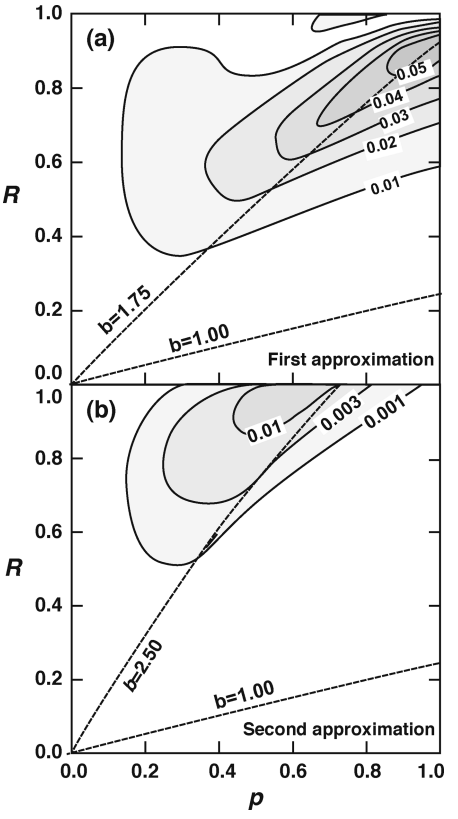

Figure 1. Contours of errors of R for the first (a) and the second (b) approximate equations. Dashed curves represent the $R-p$ relationships when $b = 1.00$, 1.75, and 2.5. The errors were obtained from the differences in R values between the approximations (the main text and Appendix B) and the numerical calculations (Appendix C).

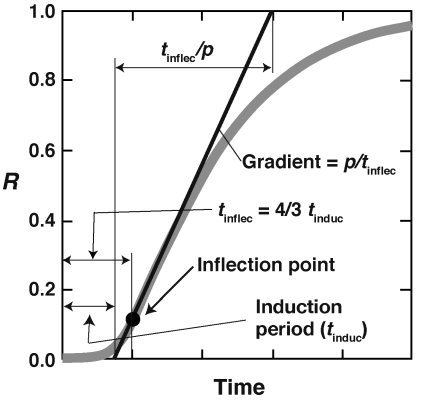

Figure 2. R variation as a function of time in the crystallization of nanoparticles. At first, R increases with the 4th power of time. Just after the inflection point, the curve shape becomes close to an exponential-type function.

$0 \le t \le t_{inflec}$, R increases approximately with the 4th power of time. This is because the volume of a crystal increases with the 3rd power of time and the number of crystals increases linearly with time. When $t = t_{inflec}$, the first nucleated crystal grows to the maximum size ($r = r_{max}$) and starts to deposit. Note that t_{inflec} ($= r_{max}/G$) is inversely proportional to G. We can calculate the value of G from the values of t_{inflec} and r_{max}. Figure 3b demonstrates that with a two-times higher growth rate, t_{inflec} becomes a half and the formation rate does not change. At the inflection point, the surface area of growing crystals (active surface area) and the transformation rate are the largest. In other words, $d^2R/dt^2 \ge 0$ when $0 \le t \le t_{inflec}$, and $d^2R/dt^2 \le 0$ when $t_{inflec} \le t$. After the inflection point, the crystallization curve becomes close to an exponential-type function, and

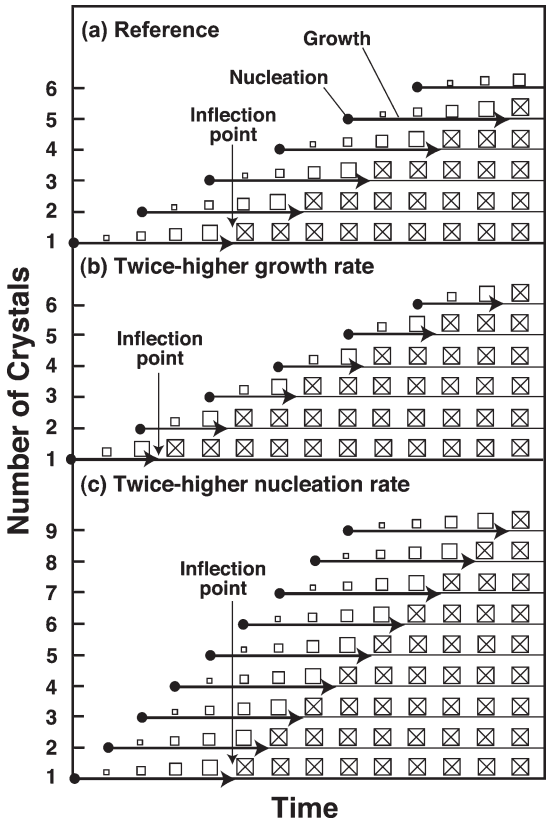

Figure 3. Schematic diagrams showing how the nucleation and growth rates affect t_{inflec} and crystallization rate: (a) a reference case, (b) the growth rate is two-times higher than the reference case, and (c) the nucleation rate is two-times higher than the reference case. The open symbols indicate growing crystals and the crossed ones indicate non-growing crystals. The figure should be read in such a way that crystal no. 1 (the number along the vertical axis) nucleates, grows, and stops growing with time; the total number of crystals at a given time can also be schematically indicated by the vertical axis. The two-times higher growth rate reduces the inflection time by half but does not change the crystallization rate (b). The two-times higher nucleation rate increases the crystallization rate by a factor of 2 (c).

the crystallization rate decreases with time (Figure 2). This is because the nucleation rate decreases as the number of nanoparticles decreases with time.

The value of dR/dt at the inflection point ($t = t_{inflec}$) is calculated from a first approximate equation (eqs 8):

$$\left|\frac{dR(t)}{dt}\right|_{t=t_{inflec}} = \frac{p}{t_{inflec}} = \frac{mI}{m_{nano}} \qquad (11)$$

Equation 11 shows that the transformation rate at the inflection point is proportional to m/m_{nano} and I. Note that the transformation rate depends on I and is independent of G. Figure 3c demonstrates that the two-times higher nucleation rate makes the formation rate two-times higher. We can conclude that the nucleation rate essentially determines the crystallization rate. Equation 11 also shows that we can calculate the value of I from the values of p/t_{inflec} and m/m_{nano}.

Figure 4 shows variations of R for different p, where the unit of time is normalized so that the gradients of R at the inflection point are one, indicating that the value of p determines the shape of R. When p is 4, the function is very close to the 4th power of time. As p decreases, t_{inflec} and $R(t_{inflec})$ decrease. When $p \leq 0.05$, t_{inflec} becomes negligible and the shape of R is close to the exponential curve ($= 1 - \exp(-pt/t_{inflec})$).

Application

Figure 5a shows the experimental data of ferrihydrite at pH 6 and 297 K by Schwertmann et al.[2] The quantities of crystals were measured with an oxalate dissolution method, and thus

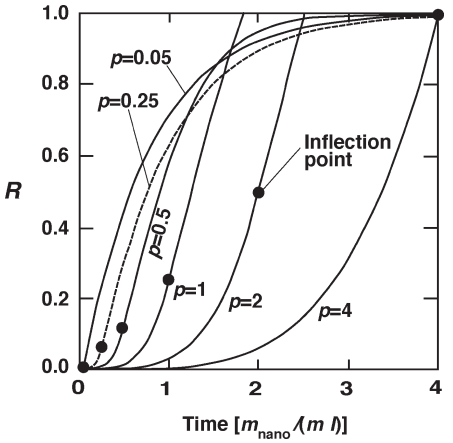

Figure 4. R for various p, where the unit of time is normalized so that the gradients of R at the inflection point are one. When p is four, the function is very close to the 4th power of time. As the p decreases, the values of t_{inflec} and $R(t_{inflec})$ decrease. When p is ≤ 0.05, the function is very close to the exponential curve [$= 1 - \exp(-pt/t_{inflec})$].

the errors of the data points will be small. The data show that R increases exponentially, and no induction period is observed. In other words, the time at the inflection point is close to zero or p is close to zero, which indicates that we can apply eq 7 to the experimental data by Schwertmann et al.[2] The value of p/t_{inflec} ($= 4.2 \times 10^{-3}$ day^{-1}) were determined from the gradient of $\ln\{1 - R(t)\}$ as described in the Theoretical Section. Substituting the value of p/t_{inflec} into eq 7, we obtain an equation, $R(t) = 1 - \exp(-4.2 \times 10^{-3}t)$ (t in days). This equation fits the experimental data excellently (solid curve in Figure 5a).

Figure 5b shows the experimental data of ferrihydrite at pH 10.7 and 361 K by Shaw et al.[5] The quantities of crystals floating in solution were directly measured with an X-ray diffraction method. This avoided the preferred orientation and reduced the errors of the measurement. The shape of the transformation curve differs from that by Schwertmann et al.;[2] the transformation curve by Shaw et al.[5] has an induction period, whereas that by Schwertmann et al.[2] does not. Figure 5b shows that nine data points shown by gray circles are fitted with a straight line. This straight line determined t_{induc} and t_{inflec} as 2.23×10^3 and 2.97×10^3 s, respectively, with a method described in the Theoretical Section. Shaw et al[5] assumed (or considered) that all ferrihydrite was finally transformed to crystals, that is, final $R = 1$ in their experiment. To re-examine their final R value, we calculated transformation curves assuming the final R value to be 1.0, 0.9, 0.8, 0.7, 0.65, and 0.6. The solid curve in Figure 5b is a transformation curve with 0.65 as a final R value and fits very well with the experimental data. We determined $p/t_{inflec} = 9.8 \times 10^{-5}$ s^{-1} from the gradient of the straight line and $p = 0.29$ from the values of t_{inflec} and p/t_{inflec}.

Figure 5c,d shows experimental data of TiO_2[19] and ZrO_2,[20] respectively. The quantities of crystals were measured with an X-ray diffraction method. Because of the preferred orientation, the errors of the data points can be larger than those by Schwertmann et al.[2] and Shaw et al.[5] The procedures to obtain calculated R variations and the parameters were as same as that for the experimental data by Shaw et al.[5] The calculated R values fit the data well for both cases. The errors of the calculated values of p and t_{inflec} will not be small because the number of the data points used for the parameter determination are small (four for TiO_2 and two for ZrO_2) and because the crystal ratios measured with an X-ray diffraction method may have errors arising from preferred orientation.

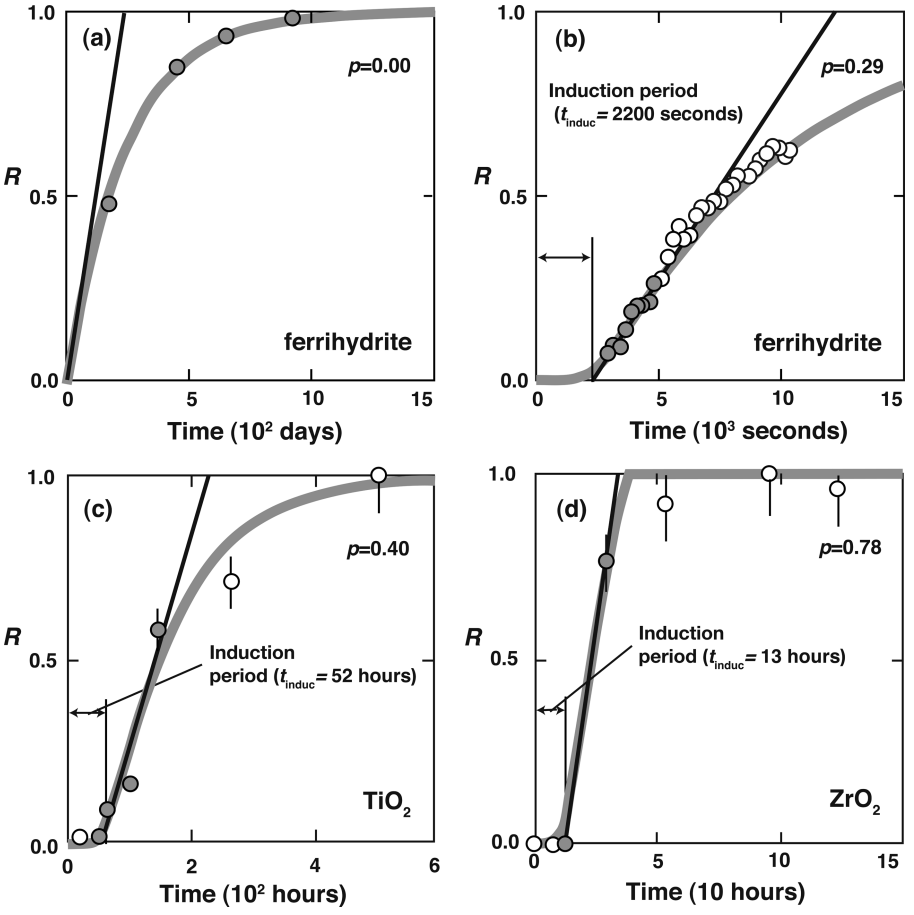

Figure 5. Relation between observed and calculated values of R: (a) the transformation of ferrihydrite at pH 6 and 297 K by Schwertmann et al.,[2] (b) the transformation of ferrihydrite at pH 10.7 and 361 K by Shaw et al.,[5] (c) the crystallization of TiO_2 at pH 1 and 473 K,[19] and (d) the crystallization of ZrO_2 at pH 0.5 and 383 K.[20] Circles denote experimental data points and solid curves calculated values based on the present theory. Data points in gray symbols were used for the determination of parameters p and t_{inflec} ($= {}^4/_3 t_{induc}$) (see Theoretical Section). We assume that errors in panels c and d are $\pm 10\%$ of R.

Discussion

Applicability of the Theory. Our theory well explains the experimental data for the transformation rates of ferrihydrite, TiO_2, and ZrO_2, including the exponential decrease of nanoparticles and the presence of induction period. This is because we have accurately described the processes of the crystallization and have made the proper assumptions.

The first assumption is that the crystals nucleate only on nanoparticles. Generally, the nucleation on a solid surface via heterogeneous nucleation is easier than homogeneous nucleation in a free space in solution, while homogeneous nucleation is possible at much higher supersaturation.[28] For example, ice dose not nucleate in a free space in air and nucleates only on clay particles or sea salts if the temperature is close to the freezing point.[29] The observation with a transmission electron microscope showed that the core of goethite formed in the transformation experiment of ferrihydrite is poorly ordered materials,[5] which implies that part of the poorly ordered materials can be ferrihydrite. Hematite forms only in the aggregates of ferrihydrite,[1] which supports the nucleation of hematite only on ferrihydrite. Therefore, the assumption of the nucleation of a crystal only on a nanoparticle is reasonable.

The second assumption is that the crystals stop growing at a certain size. This was also assumed in the theory of Zhang et al. on the basis of the observation of TiO_2 crystals.[27] Transformation experiments of ferrihydrite nanoparticles showed that most hematite and goethite crystals are about 50 to 100 nm in size.[2] This also suggests that these crystals stop growing at about 50−100 nm. This seems to be related to the deposition of crystals; particles of goethite or hematite larger than 50 nm can deposit, but particles less than 50 nm float in solution, which will be well explained by our calculations that consider the experimental conditions of Schwertmann et al.[2] The calculated results are shown in Figure 6a,b for the depth distributions of particles as a function of diameter in equilibrium in 100- and 1-mm height solutions, respectively, and in Figure 6c for the time required for a particle to fall by 1, 10, and 100 mm in solution assuming that the density of particles is 4.3 (the density of goethite). The equilibrium depth distribution of particles obeys the Boltzmann distribution, and the fall rate of a particle obeys the Stokes' law. When the diameters of particles are less than 10 nm (Figure 6a) and 50 nm (Figure 6b), the particles are homogeneously distributed throughout solutions, and the particles never deposit at the bottom. Therefore, the particles less than 10 nm in diameter can continue to grow in a bottle of 100 mm height, and the particles less than 50 nm can do so in a bottle of 1 mm height. On the other hand, 99% of particles are present within the lower 1 mm depth for particles of 100 nm in diameter in solution with 100 mm height (Figure 6a). Particles of 100 nm in diameter fall by 100 mm in 73 days (Figure 6c). Consequently, our calculations well explain why the crystal size given by Schwertmann et al.[2] is less than 100 nm. On the other hand, the crystals for the transformation experiment by Shaw et al.[5] are 1 order of magnitude

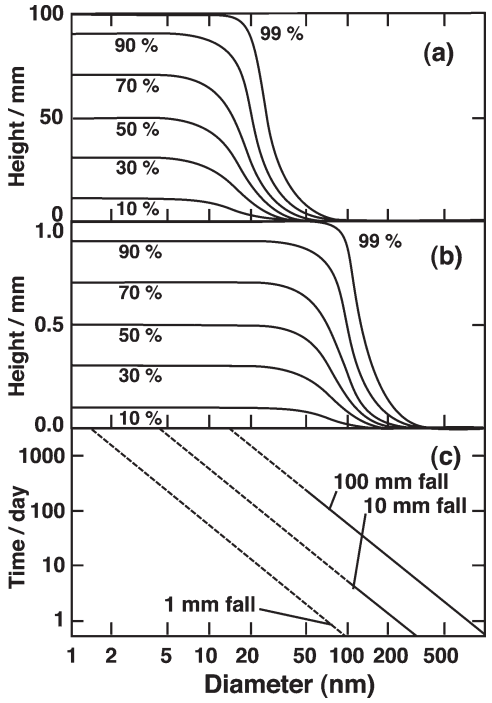

Figure 6. (a, b) Depth distribution of crystal (goethite) as a function of particle size in equilibrium in 10- and 1-mm height solutions, respectively. The percent values with the curves in panels a and b represent upper limits of abundance ratios of particles, for example, the 50% curve shows that 50% of particles are present below the curve. The curves indicate that the particles are homogeneously distributed throughout a solution when particles are < 10 nm in diameter. (c) Time needed for a goethite particle to fall by 1, 10, and 100 mm in solution as a function of particle size. The dashed lines in panel c show that a particle does not fall by a given depth, for example, particles of < 100 nm never fall by 10 mm.

larger than those by Schwertmann et al.[2] Schwertmann et al.[2] did not stir the solution, and their sampling interval was a few hundred days. In contrast, Shaw et al.[5] stirred the solution, and their experimental periods were shorter, which prevented the deposit of small crystals and made crystals grow larger in the solution.

The third assumption is that X_{sol} (the concentration of M in solution) is close to $X_{nano\text{-}eq}$ (the solubility of nanoparticle). Giving an example for the transformation of ferrihydrite, we demonstrate that this assumption is valid. The assumption is deducted from dissolution rates and surface areas of nanoparticles and crystals using the relation

$$J_{nano\text{-}dissol} = J_{format} \tag{12}$$

If X_{sol} is zero, eq 12 is valid. When $X_{nano\text{-}eq}$ is small, $J_{nano\text{-}dissol}$ becomes approximately equal to J_{format} in very short time (Appendix D). The formation rate of crystals and the dissolution rate of nanoparticles are given by

$$\begin{aligned} J_{format} &= kS(X_{sol} - X_{eq}) \\ J_{nano\text{-}dissol} &= k_{nano}S_{nano}(X_{nano\text{-}eq} - X_{sol}) \end{aligned} \tag{13}$$

where $J_{dissol} = -J_{format}$. Note that the surface area of crystals that stop growing is not included in S. When both crystals and nanoparticles are dissolved in pure water, the dissolution rates of crystals and nanoparticles are given by

$$\begin{aligned} J_{dissol} &= kSX_{eq} \\ J_{nano\text{-}dissol} &= k_{nano}S_{nano}X_{nano\text{-}eq} \end{aligned} \tag{14}$$

The dissolution experiments of ferrihydrite, goethite, and hematite in pure water show that the ratio of $(J_{nano\text{-}dissol}/S_{nano})/(J_{dissol}/S)$ is in the range between 8.8×10 and 2.4×10^3.[30] The calculation based on the thermodynamic database by Naumov et al.[31] shows that the ratio of $X_{nano\text{-}eq}/X_{eq}$ is 200 when the nanoparticle is ferrihydrite and the crystal is goethite. In this case, k_{nano}/k is in the range between 0.88 and 12. Using eqs 12 and 13, we obtain the relation

$$\begin{aligned} 0.88(S_{nano}/S) < (X_{sol} - X_{eq})/(X_{nano\text{-}eq} - X_{sol}) \\ < 12(S_{nano}/S) \end{aligned} \tag{15}$$

Because S_{nano}/S is larger than 28.0 for the transformation of ferrihydrite when $p \leq 0.5$ (Appendix E), $(X_{sol} - X_{eq})/(X_{nano\text{-}eq} - X_{sol})$ is larger than 24.6, and therefore, X_{sol} is approximately equal to $X_{nano\text{-}eq}$, which is the third assumption.

The relation of the activation energies between nucleation and crystal growth, which are determined on the basis of the theory, also supports the validity of the theory. The theory indicates that the inflection time ($t_{inflec} = r_{max}/G$) is inversely proportional to the crystal growth rate (G), and that $dR(t_{inflec})/dt$ (the gradient of the transformation curve at the inflection point) is proportional to I (nucleation rate coefficient). From these relations, we have re-interpreted the experimental results of the transformation of ferrihydrite[5] and have obtained the reasonable result that the activation energy for nucleation is larger than that for crystal growth, which is consistent with the relation of activation energies between nucleation and crystal growth for condensed matter.[32,33]

Relation to Other Theories. Our theory is closely related to the Avrami theory[24−26] and the theory by Zhang et al.[27] The Avrami theory is applied to the transformation rate of metastable to stable phases and considers two processes, nucleation and growth of nuclei. The shapes of the transformation curves of Avrami theory resemble those of the present theory. The R values can be approximated by the 4th power of time in the initial state and, later, by exponential-type functions for both theories. The Avrami equation is, however, derived for the transformation of condensed matter such as glass, amorphous alloy, and melt, and it cannot be applied to the transformation of nanoparticles in solution. Although the Avrami equation $[1 - \exp(-kt^n)]$ can fit experimental data for the transformation of ferrihydrite as is shown by Yee et al.[7] by changing the parameter n, the meaning of the value of n (for example, 1.55 to 1.81 in Yee et al.[7] is unclear. The theory by Zhang et al. has been proposed for the crystallization of nanoparticles in dry system and successfully explains the crystallization of TiO_2 nanoparticles.[27] This theory assumes that a crystal grows to a maximum size in a very short time and thus cannot explain the presence of induction period. On the other hand, we have successfully explained the presence of induction period by taking account of the effects of both nucleation and growth rates. Our theory shows that the induction period is observed when the growth of the crystal is slow compared with nucleation.

Prediction by the Present Theory. We have shown that the rate-determining process of crystallization of nanoparticles in solution is the nucleation of crystals, not the growth rate of crystals (eq 11). Therefore, the effects of temperature, pH, and impurities on nucleation rate are more important than those on growth rate. Some impurities, such as organic matter,[34,35] silicon,[36] phosphate,[5,37] and cadmium,[38] decrease the transformation rate of ferrihydrite, while the presence of divalent iron increases the transformation rate;[7] impurities can retard or enhance the nucleation of crystals.

Note that the transformation is retarded or enhanced by impurities in solution but not in nanoparticles. Therefore, we can stabilize nanoparticles by adding some kind of impurity to the solution.

The value of p will increase with increasing temperature. This is because the activation energy of nucleation will be larger than that of crystal growth. This means that the value of I/G increases with increasing temperature. Therefore, the value of p [$= (I/G)r_{max}(m/m_{nano})$] will be large at high temperatures. As a result, an induction period may be observed at high temperatures even if no induction period is observed at room temperature.

Some nonthermodynamic parameters such as the turbulence of solution and the height of a bottle affect the transformation rate of nanoparticles to crystals. If we stir a solution as in the experiments by Shaw et al.[5] and Yee et al.,[7] the transformation rate increases because the high turbulence of the solution prevents crystals from depositing and makes crystals stay in the solution and grow larger. Consequently, the values of r_{max} and m become larger, which in turn makes the induction period and the transformation rate larger because $t_{induc} = {}^3/_4 t_{inflec} = {}^3/_4 r_{max}/G$ and $dR/dt = (m/m_{nano})I$ when $t = t_{inflec}$. In fact, the crystals formed in the experiments with stirring[5] are 1 order of magnitude larger than the crystals formed in the experiments without stirring.[2] If a crystal grows 10 times larger in diameter with stirring than a crystal doeswithout stirring, the transformation rate with stirring becomes a thousand times higher than that without stirring. The height of the bottle may also affect the transformation rate. Crystals 100 nm in diameter deposit in a bottle with a height of 100 mm, but the crystals can float in a solution with a height of 1 mm (Figures 5a,b, respectively). Therefore, crystals in a short bottle can grow to large sizes, and thus the crystallization rate is high for crystals in a short bottle. Consequently, the theory shows that we should stir a solution when we need to synthesize large crystals and that we should use a tall bottle when we need to synthesize small crystals.

Formation of Nanoparticles. We have shown that heterogeneous nucleation (nucleation on nanoparticles) is important for the crystallization of nanoparticles. Then, a question arises how nanoparticles nucleate when no particle exists in solution. These nanoparticles must nucleate homogeneously. The homogeneous nucleation needs high supersaturation. For example, amorphous silica requires 30% excess of equilibrium for homogeneous nucleation, and quartz requires a supersaturation of a factor of 80.[28] Ferrihydrite nanoparticles were also formed from a highly supersaturated solution.[2] The nucleation rate is very fast when the concentration is higher than a critical point, but nanoparticles hardly nucleate when the concentration is lower than the critical point.[28] Therefore, nucleation of nanoparticles can be completed in a short time in a highly supersaturated solution. For example, the formation of ferrihydrite nanoparticles is completed in less than 5 min.[35] Once nanoparticles form, the concentration in the solution will decrease to become close to the solubility of the nanoparticle as a result of the growth of nanoparticles.

Conclusions

The present kinetic theory of the crystallization of nanoparticles has been developed assuming the following: (i) crystals nucleate only on nanoparticles, (ii) the crystals stop growing at a certain size, and (iii) the concentration of metal of the nanoparticles in solution is close to the solubility of the nanoparticles. Our theory explains the crystallization rates of reported experiments excellently including the exponential decrease of nanoparticles and the presence of an induction period. The calculated results are also consistent with other experimental data such as the size of crystals and the dissolution rates of nanoparticles and crystals.

The crystallization rate of nanoparticles in solution is proportional to the nucleation rate of crystals and is independent of the growth rate of crystals. On the other hand, the induction period is inversely proportional to the growth rate of crystals.

Some nonthermodynamic parameters such as the turbulence of solution and the size of system can also affect the crystallization rate. For example, the stirring of solution prevents crystals from depositing and makes the crystals grow larger, which in turn makes the crystallization rate higher.

Acknowledgment. This work was partly supported by a Grant-in-Aid of the Ministry of Education, Culture, Sports, Science and Technology to T.M.

Appendix A

We here derive the integral equations for R and their differentials. As shown in the text, the total volume of crystals nucleating between time τ and $\tau + d\tau$ is given by

$$\begin{aligned} dV &= \frac{4\pi}{3}\{(t-\tau)G\}^3 I N_{nano}(\tau)\, d\tau \quad (t-\tau \le t_{inflec}) \\ dV &= \frac{4\pi}{3}(r_{max})^3 I N_{nano}(\tau)\, d\tau \quad (t-\tau \ge t_{inflec}) \end{aligned} \tag{A1}$$

Integrating dV from 0 to t, we obtain the total volume of crystals:

$$\begin{aligned} V(t) &= \int_0^t \frac{4\pi}{3}\{(t-\tau)G\}^3 I N_{nano}(\tau)\, d\tau \quad (t \le t_{inflec}) \\ V(t) &= \int_0^{t-t_{inflec}} \frac{4\pi}{3}(t_{inflec}G)^3 I N_{nano}(\tau) I\, d\tau \\ &+ \int_{t-t_{inflec}}^{t} \frac{4\pi}{3}\{(t-\tau)G\}^3 I N_{nano}(\tau) I\, d\tau \quad (t_{inflec} \le t) \end{aligned} \tag{A2}$$

With conversion of the time parameters with $t = t_{inflec}b$ and $\tau = t_{inflec}\beta$, the volume of total crystals is given by

$$\begin{aligned} &V(t_{inflec}b) \\ &= v_{max} t_{inflec} I \int_0^b (b-\beta)^3 N_{nano}(t_{inflec}\beta)\, d\beta \quad (b \le 1) \\ &V(t_{inflec}b) = v_{max} t_{inflec} I \Big[\int_0^{b-1} N_{nano}(t_{inflec}\beta)\, d\beta \\ &+ \int_{b-1}^{b} (b-\beta)^3 N_{nano}(t_{nano}\beta)\, d\beta\Big] \quad (b \ge 1) \end{aligned} \tag{A3}$$

Because $R + R_{nano} = 1$ and all metal is in nanoparticles initially, R is given by

$$\begin{aligned} R(t_{inflec}b) &= \frac{M(t_{inflec}b)}{M_{nano}(0)} = \frac{V(t_{inflec}b)/v}{N_{nano}(0)m_{nano}} \\ &= \frac{V(t_{inflec}b)/(v_{max}/m)}{N_{nano}(0)m_{nano}} = \frac{m}{N_{nano}(0)m_{nano}v_{max}} V(t_{inflec}b) \end{aligned} \tag{A4}$$

Substituting eq A3 into eq A4, we obtain the following equations:

$$\begin{aligned} R(t_{\mathrm{inflec}}b) &= p\int_0^b (b-\beta)^3 R_{\mathrm{nano}}(t_{\mathrm{inflec}}\beta)\,\mathrm{d}\beta \qquad (b\le 1)\\ &= p\int_0^b (b-\beta)^3[1-R(t_{\mathrm{inflec}}\beta)]\,\mathrm{d}\beta\\ R(t_{\mathrm{inflec}}b) &= p[\int_0^{b-1} R_{\mathrm{nano}}(t_{\mathrm{inflec}}\beta)\,\mathrm{d}\beta\\ &\quad + \int_{b-1}^b (b-\beta)^3 R_{\mathrm{nano}}(t_{\mathrm{inflec}}\beta)\,\mathrm{d}\beta] \quad (b\ge 1)\\ &= p[\int_0^{b-1}\{1-R(t_{\mathrm{inflec}}\beta)\}\,\mathrm{d}\beta\\ &\quad + \int_{b-1}^b (b-\beta)^3\{1-R(t_{\mathrm{inflec}}\beta)\}\,\mathrm{d}\beta] \qquad \text{(A5)} \end{aligned}$$

where $p = It_{\mathrm{inflec}}m/m_{\mathrm{nano}} = (I/G)(m/m_{\mathrm{nano}})r_{\max}$.

Next, we derive the differential of R. We here derive the differentiation from the active surface area (the surface area of growing crystals). The active surface area of crystals nucleating between time τ and $\tau + \mathrm{d}\tau$ is given by

$$\begin{aligned} \mathrm{d}S &= 4\pi I\{(t-\tau)G\}^2\,\mathrm{d}\tau \quad (t-\tau\le t_{\mathrm{inflec}})\\ \mathrm{d}S &= 0 \quad (t-\tau\ge t_{\mathrm{inflec}}) \end{aligned} \qquad \text{(A6)}$$

Integrating $\mathrm{d}S$ from 0 to t, we obtain the active surface area of crystals:

$$\begin{aligned} S(t) &= \int_0^t 4\pi\{(t-\tau)G\}^2 N_{\mathrm{nano}}(\tau) I\,\mathrm{d}\tau \qquad (t\le t_{\mathrm{inflec}})\\ S(t) &= \int_{t-t_{\mathrm{inflec}}}^t 4\pi\{(t-\tau)G\}^2 N_{\mathrm{nano}}(\tau) I\,\mathrm{d}\tau \quad (t_{\mathrm{inflec}}\le t) \end{aligned} \qquad \text{(A7)}$$

Converting the time parameters with $t = t_{\mathrm{inflec}}b$ and $\tau = t_{\mathrm{inflec}}\beta$ gives the active surface area as

$$\begin{aligned} S(t_{\mathrm{inflec}}b) &= 4\pi(r_{\max})^2 t_{\mathrm{inflec}} I\int_0^b (b-\beta)^2\times \qquad (b\le 1)\\ &\quad N_{\mathrm{nano}}(t_{\mathrm{inflec}}\beta)\,\mathrm{d}\beta\\ &= 4\pi(r_{\max})^2 t_{\mathrm{inflec}} I\int_0^b \{(b-\beta)^2\times\\ &\quad M_{\mathrm{nano}}(t_{\mathrm{inflec}}\beta)/m_{\mathrm{nano}}\}\,\mathrm{d}\beta\\ &= 4\pi(r_{\max})^2 t_{\mathrm{inflec}} I\int_0^b \{(b-\beta)^2\times\\ &\quad R_{\mathrm{nano}}(t_{\mathrm{inflec}}\beta)M_{\mathrm{nano}}(0)/m_{\mathrm{nano}}\}\,\mathrm{d}\beta\\ &= 4\pi(r_{\max})^2 t_{\mathrm{inflec}} I M_{\mathrm{nano}}(0)/m_{\mathrm{nano}}\times\\ &\quad \int_0^b (b-\beta)^2 R_{\mathrm{nano}}(t_{\mathrm{inflec}}\beta)\,\mathrm{d}\beta\\ S(t_{\mathrm{inflec}}b) &= 4\pi(r_{\max})^2 t_{\mathrm{inflec}} I\int_{b-1}^b (b-\beta)^2\times \qquad (b\ge 1)\\ &\quad N_{\mathrm{nano}}(t_{\mathrm{inflec}}\beta)\,\mathrm{d}\beta\\ &= 4\pi(r_{\max})^2 t_{\mathrm{inflec}} I\int_{b-1}^b \{(b-\beta)^2\times\\ &\quad M_{\mathrm{nano}}(t_{\mathrm{inflec}}\beta)/m_{\mathrm{nano}}\}\,\mathrm{d}\beta\\ &= 4\pi(r_{\max})^2 t_{\mathrm{inflec}} I\int_{b-1}^b \{(b-\beta)^2\times\\ &\quad R_{\mathrm{nano}}(t_{\mathrm{inflec}}\beta)M_{\mathrm{nano}}(0)/m_{\mathrm{nano}}\}\,\mathrm{d}\beta\\ &= 4\pi(r_{\max})^2 t_{\mathrm{inflec}} I M_{\mathrm{nano}}(0)/m_{\mathrm{nano}}\times\\ &\quad \int_{b-1}^b (b-\beta)^2 R_{\mathrm{nano}}(t_{\mathrm{inflec}}\beta)\,\mathrm{d}\beta \end{aligned} \qquad \text{(A8)}$$

The differentiation of R is given by

$$\begin{aligned} \frac{\mathrm{d}R(t_{\mathrm{inflec}}b)}{\mathrm{d}b} &= t_{\mathrm{inflec}}\frac{\mathrm{d}R(t)}{\mathrm{d}t} = \frac{t_{\mathrm{inflec}}}{M_{\mathrm{nano}}(0)}\frac{\mathrm{d}M_{\mathrm{nano}}(t)}{\mathrm{d}t}\\ &= \frac{t_{\mathrm{inflec}}}{M_{\mathrm{nano}}(0)v}\frac{\mathrm{d}V(t)}{\mathrm{d}t} = \frac{t_{\mathrm{inflec}}}{M_{\mathrm{nano}}(0)v}\frac{\mathrm{d}V(t)}{\mathrm{d}r}\frac{\mathrm{d}r}{\mathrm{d}t}\\ &= \frac{t_{\mathrm{inflec}}}{M_{\mathrm{nano}}(0)v}S(t)G = \frac{r_{\max}}{M_{\mathrm{nano}}(0)v}S(t) \end{aligned} \qquad \text{(A9)}$$

By substituting eq A8 into eq A9, we obtain

$$\begin{aligned} \frac{\mathrm{d}R(t_{\mathrm{inflec}}b)}{\mathrm{d}b} &= 3p\int_0^b (b-\beta)^2 R_{\mathrm{nano}}(t_{\mathrm{inflec}}\beta)\,\mathrm{d}\beta \qquad (b\le 1)\\ &= 3p\int_0^b (b-\beta)^2[1-R(t_{\mathrm{inflec}}\beta)]\,\mathrm{d}\beta\\ \frac{\mathrm{d}R(t_{\mathrm{inflec}}b)}{\mathrm{d}b} &= 3p\int_{b-1}^b (b-\beta)^2 R_{\mathrm{nano}}(t_{\mathrm{inflec}}\beta)\,\mathrm{d}\beta \qquad (b>1)\\ &= 3p\int_{b-1}^b (b-\beta)^2[1-R(t_{\mathrm{inflec}}\beta)]\,\mathrm{d}\beta \end{aligned} \qquad \text{(A10)}$$

Appendix B

We here derive the second approximate equations using integral eqs 2 and 8. When calculating the equations, we divide the values of b into three ranges ($0 \le b \le 1$, $1 \le b \le 2$, and $2 \le b$). When $0 \le b \le 1$, by substituting the first equation of eqs 8 into R of the right-hand of the first equation of eqs 2, we obtain the second approximation equation:

$$\begin{aligned} R_2 &= p\int_0^b (b-\beta)^3\left(1-\frac{p}{4}\beta^4\right)\mathrm{d}\beta = p\int_0^b (b-\beta)^3\,\mathrm{d}\beta\\ &\quad -\frac{p^2}{4}\int_0^b \beta^4(b-\beta)^3\,\mathrm{d}\beta = p\left[-\frac{(b-\beta)^4}{4}\right]_0^b\\ &\quad -\frac{p^2}{4}\left[\frac{b^3\beta^5}{5}-\frac{b^2\beta^6}{2}+\frac{3b\beta^7}{7}-\frac{\beta^8}{8}\right]_0^b = \frac{pb^4}{4}-\frac{p^2b^8}{1120} \end{aligned} \qquad \text{(B1)}$$

When $1 \le b \le 2$, by substituting the eqs 8 into R of the right-hand of the second equation of eqs 2, we obtain the second approximate equation:

$$\begin{aligned} R_2 &= p\left[\int_0^{b-1}\left(1-\frac{p}{4}\beta^4\right)\mathrm{d}\beta + \int_{b-1}^1 (b-\beta)^3\left(1-\frac{p}{4}\beta^4\right)\mathrm{d}\beta\right.\\ &\quad \left. + \int_1^b (b-\beta)^3\left\{1-p\left(b-\frac{3}{4}\right)\right\}\mathrm{d}\beta\right] \end{aligned} \qquad \text{(B2)}$$

The first term in the parentheses of eq B2 is calculated to be

$$\int_0^{b-1}\left(1-\frac{p}{4}\beta^4\right)\mathrm{d}\beta = \left[\beta-\frac{p}{20}\beta^5\right]_0^{b-1} = (b-1)-\frac{p}{20}(b-1)^5 \qquad \text{(B3)}$$

The second term in the parentheses of eq B2 is calculated to be

$$\begin{aligned} \int_{b-1}^1 (b-\beta)^3\left(1-\frac{p}{4}\beta^4\right)\mathrm{d}\beta &= \int_{b-1}^1 (b-\beta)^3\,\mathrm{d}\beta\\ &\quad -\frac{p}{4}\int_{b-1}^1 \beta^4(b-\beta)^4\,\mathrm{d}\beta = \left[-\frac{(b-\beta)^4}{4}\right]_{b-1}^1\\ &\quad -\frac{p}{4}\left[\frac{b^3\beta^5}{5}-\frac{b^2\beta^6}{2}+\frac{3b\beta^7}{7}-\beta^7\right]_{b-1}^1 = \frac{1}{4}\{1-(b-1)^4\}\\ &\quad -\frac{p}{4}\left(-\frac{b^8}{280}+\frac{b^4}{4}-\frac{3b^3}{5}+\frac{b^2}{2}-\frac{b}{7}\right) \end{aligned} \qquad \text{(B4)}$$

The third term in the parentheses of eq B2 is calculated to be

$$\begin{aligned}\int_1^b (b-\beta)^3\left\{1-p\left(b-\frac{3}{4}\right)\right\}\mathrm{d}\beta &= \left(1+\frac{3p}{4}-pb\right)\int_1^b (b-\beta)^3\,\mathrm{d}\beta + p\int_1^b (b-\beta)^4\,\mathrm{d}\beta \\ &= \left(1+\frac{3p}{4}-pb\right)\left[-\frac{(b-\beta)^4}{4}\right]_1^b + p\left[-\frac{(b-\beta)^5}{5}\right]_1^b \\ &= \frac{(b-1)^4}{4} - \frac{p}{80}(4b^5-15b^4+20b^3-10b^2+1) \qquad \text{(B5)}\end{aligned}$$

Substituting eqs B3, B4, and B5 into eq B2, we obtain the second approximate equation ($1 \le b \le 2$):

$$R_2 = p\left(b-\frac{3}{4}\right) + \frac{p^2}{1120}(b^8-112b^5+420b^4-672b^3+560b^2-240b+42) \qquad \text{(B6)}$$

When $2 \le b$, by substituting eqs 8 into R of the right-hand of the second equation of eqs 2, we obtain the second approximate equation:

$$\begin{aligned}R_2 &= p\left[\int_0^1 \left(1-\frac{p}{4}\beta^4\right)\mathrm{d}\beta + \int_1^{b-1}\left\{1-p\left(\beta-\frac{3}{4}\right)\right\}\mathrm{d}\beta + \int_{b-1}^b (b-\beta)^3\left\{1-p\left(\beta-\frac{3}{4}\right)\right\}\mathrm{d}\beta\right] \\ &= p\left[\int_0^1 \left(1-\frac{p}{4}\beta^4\right)\mathrm{d}\beta + \int_1^{b-1}\left\{1+\frac{3p}{4}-p\beta\right\}\mathrm{d}\beta + \int_{b-1}^b \left\{\left(1+\frac{3}{4}p-pb\right)(b-\beta)^3 + p(b-\beta)^4\right\}\mathrm{d}\beta\right] \\ &= p\left\{\left[\beta-\frac{p}{20}\beta^5\right]_0^1 + \left[\left(1+\frac{3p}{4}\right)\beta-\frac{p\beta^2}{2}\right]_1^{b-1} + \left[-\left(1+\frac{3}{4}p-pb\right)\frac{(b-\beta)^4}{4} - p\frac{(b-\beta)^5}{5}\right]_{b-1}^b\right\} \\ &= p\left\{-\frac{p}{20}+1+\frac{p(-2b^2+7b-6)}{4}+b-2+\frac{p}{80}(-20b+31)+\frac{1}{4}\right\} \\ &= p\left(b-\frac{3}{4}\right)+\frac{p^2}{80}(-40b^2+120b-93) \qquad \text{(B7)}\end{aligned}$$

In summary, the second approximate equations for $0 \le b \le 2.5$ are

$$\begin{aligned}R_2 &= \frac{pb^4}{4}-\frac{p^2b^8}{1120} \qquad (0\le b\le 1) \\ R_2 &= p\left(b-\frac{3}{4}\right)+\frac{p^2}{1120}(b^8-112b^5+420b^4-672b^3+560b^2-240b+42) \qquad (1\le b\le 2) \\ R_2 &= p\left(b-\frac{3}{4}\right)+\frac{p^2}{80}(-40b^2+120b-93) \qquad (2\le b\le 2.5)\end{aligned} \qquad \text{(B8)}$$

We did not calculate the third approximate equations because the second approximate equations are accurate enough for small b values and because higher orders of approximate equations are not accurate enough for large b values, either, and are too complicated.

For b values larger than 2.5, we approximate R with an exponential-type function:

$$R_2 = 1 - A\exp[-B(b-2.5)] \qquad (2.5\le b) \qquad \text{(B9)}$$

The parameters A and B are determined so as to connect smoothly with eqs B8 at 2.5 of b. As a result, we have obtained the values of the parameters as follows:

$$\begin{aligned}A &= 0.5375p^2-1.75p+1 \\ B &= \frac{-p^2+p}{0.5375p^2-1.75p+1}\end{aligned} \qquad \text{(B10)}$$

Appendix C

We here show how the R values are calculated numerically. The differential of R is given by

$$\begin{aligned}\frac{\mathrm{d}R(t_{\mathrm{inflec}}b)}{\mathrm{d}b} &= 3p\int_0^b (b-\beta)^2[1-R(t_{\mathrm{inflec}}\beta)]\,\mathrm{d}\beta \qquad (0\le b\le 1) \\ \frac{\mathrm{d}R(t_{\mathrm{inflec}}b)}{\mathrm{d}b} &= 3p\int_{b-1}^b (b-\beta)^2[1-R(t_{\mathrm{inflec}}\beta)]\,\mathrm{d}\beta \qquad (1\le b)\end{aligned} \qquad \text{(C1)}$$

See Appendix A for the derivation of eqs C1. Replacing $b = m/n$ (m and n are integers), eqs C1 are approximated to

$$\begin{aligned}&\frac{\mathrm{d}R(t_{\mathrm{inflec}}\,m/n)}{\mathrm{d}b} \\ &= 3p\left(\frac{1}{n}\right)\sum_{i=1}^{m}\left[\left(\frac{m}{n}-\frac{i-0.5}{n}\right)^2\left\{1-R\left(t_{\mathrm{inflec}}\frac{i-0.5}{n}\right)\right\}\right] \quad (m\le n) \\ &\frac{\mathrm{d}R(t_{\mathrm{inflec}}\,m/n)}{\mathrm{d}b} \\ &= 3p\left(\frac{1}{n}\right)\sum_{i=m-n+1}^{m}\left[\left(\frac{m}{n}-\frac{i-0.5}{n}\right)^2\left\{1-R\left(t_{\mathrm{inflec}}\frac{i-0.5}{n}\right)\right\}\right] \quad (m\ge n)\end{aligned} \qquad \text{(C2)}$$

On the other hand, the value of $R(t_{\mathrm{inflec}}(m+0.5)/n)$ can be calculated from the values of $R(t_{\mathrm{inflec}}(m-0.5)/n)$ and $\mathrm{d}R(t_{\mathrm{inflec}}m/n)/\mathrm{d}b$ with the following equation:

$$R(t_{\mathrm{inflec}}(m+0.5)/n) = R(t_{\mathrm{inflec}}(m-0.5)/n) + \frac{1}{n}\frac{\mathrm{d}R(t_{\mathrm{inflec}}m/n)}{\mathrm{d}b} \qquad \text{(C3)}$$

The value of $R(0.5t_{\mathrm{inflec}}/n)$ is set to zero. Using eqs C2 and C3 alternately, we have calculated the values of R and $\mathrm{d}R/\mathrm{d}b$ step by step. Table C1 shows the values of R calculated with a program made on an EXCEL sheet. We can obtain the values of R accurately with this method if n is large enough; errors of R calculated with this method are less than 0.003 and 0.0001 for $n = 10$ and 50, respectively. Theses errors were estimated from the difference of R between $n = 10$ and 50. Because the deviation from a true value is inversely proportional to n^2, the deviation for the calculation with $n = 10$ is 25 times larger than that with $n = 50$. This means that the difference of R between $n = 10$ and $n = 50$ is 24 times larger than the deviation of the calculation with $n = 50$. We can obtain the deviation from a true value for $n = 50$ and $n = 10$ by dividing the difference of R between $n = 10$ and 50 by 24 and 25/24, respectively.

Appendix D

We show here that J_{format} can be very close to $J_{\mathrm{nano\text{-}dissol}}$ in a short time. The degree of closeness between J_{format} and

Table C1. Numerically Calculated R Values for $n = 10$ and $n = 50$

	R								
	$p = 0.2$			$p = 0.5$			$p = 1.0$		
b	$n = 10$	$n = 50$	diff.	$n = 10$	$n = 50$	diff.	$n = 10$	$n = 50$	diff.
0.15	0.00001	0.00002	−0.00001	0.00004	0.00006	−0.00002	0.00008	0.00012	−0.00005
0.25	0.00016	0.00019	−0.00003	0.00041	0.00049	−0.00007	0.00082	0.00097	−0.00015
0.35	0.00069	0.00075	−0.00006	0.00172	0.00187	−0.00014	0.00345	0.00374	−0.00029
0.45	0.00195	0.00205	−0.00010	0.00487	0.00512	−0.00024	0.00975	0.01023	−0.00048
0.55	0.00442	0.00457	−0.00014	0.01106	0.01142	−0.00036	0.02212	0.02284	−0.00072
0.65	0.00871	0.00892	−0.00020	0.02178	0.02229	−0.00050	0.04355	0.04456	−0.00101
0.75	0.01554	0.01581	−0.00027	0.03883	0.03950	−0.00067	0.07762	0.07896	−0.00134
0.85	0.02573	0.02608	−0.00034	0.06429	0.06515	−0.00086	0.12848	0.13019	−0.00171
0.95	0.04025	0.04068	−0.00043	0.10055	0.10162	−0.00107	0.20083	0.20295	−0.00212
1.05	0.06018	0.05996	0.00022	0.15025	0.14969	0.00056	0.29989	0.29873	0.00116
1.15	0.08007	0.07990	0.00017	0.19979	0.19934	0.00045	0.39829	0.39731	0.00097
1.25	0.09992	0.09979	0.00013	0.24904	0.24869	0.00035	0.49555	0.49473	0.00081
1.35	0.11970	0.11961	0.00008	0.29784	0.29758	0.00026	0.59098	0.59030	0.00068
1.45	0.13936	0.13932	0.00004	0.34594	0.34577	0.00017	0.68365	0.68309	0.00056
1.55	0.15888	0.15888	−0.00000	0.39307	0.39298	0.00008	0.77243	0.77198	0.00046
1.75	0.19721	0.19730	−0.00009	0.48306	0.48315	−0.00010	0.93303	0.93282	0.00021
2.05	0.25222	0.25246	−0.00023	0.60260	0.60308	−0.00048			
2.55	0.33616	0.33663	−0.00047	0.75475	0.75584	−0.00109			
3.05	0.41082	0.41149	−0.00066	0.85535	0.85677	−0.00142			
4.05	0.54690	0.54783	−0.00093	0.96014	0.96139	−0.00126			
5.05	0.64314	0.64417	−0.00103						
6.05	0.71893	0.71998	−0.00105						
7.05	0.77863	0.77964	−0.00101						
8.05	0.82143	0.82238	−0.00095						
9.05	0.85936	0.86022	−0.00086						
10.05	0.88923	0.89000	−0.00077						

$J_{\text{nano-dissol}}$ is expressed by the equation

$$D_{\text{close}} = \frac{|J_{\text{format}} - J_{\text{nano-dissol}}|}{J_{\text{nano-dissol}}} \tag{D1}$$

Using eq D1, we can calculate the time needed for attaining a small D_{close} value (for example, $D_{\text{close}} = 0.01$).

First, we derive a function of $X_{\text{sol}}(t)$. The differentiation of $X_{\text{sol}}(t)$ is given by

$$\begin{aligned}\frac{dX_{\text{sol}}(t)}{dt} &= -\frac{dX_{\text{nano}}}{dt} - \frac{dX}{dt} = -k_{\text{nano}}S_{\text{nano}}(X_{\text{sol}}(t) \\ &- X_{\text{nano-eq}}) - kS(X_{\text{sol}}(t) - X_{\text{eq}}) \\ &= -(k_{\text{nano}}S_{\text{nano}} + kS)X_{\text{sol}}(t) + k_{\text{nano}}S_{\text{nano}}X_{\text{nano-eq}} + kSX_{\text{eq}}\end{aligned} \tag{D2}$$

Solving differential eq D2, we obtain the equation

$$\begin{aligned}X_{\text{sol}}(t) = (X_{\text{sol}}(t_0) - X_{\text{steady}})\exp[-(k_{\text{nano}}S_{\text{nano}} \\ + kS)(t - t_0)] + X_{\text{steady}}\end{aligned} \tag{D3}$$

where $X_{\text{sol}}(t_0)$ and X_{steady} are the concentrations of metal in solution in the initial and steady states, respectively, and $X_{\text{steady}} = (k_{\text{nano}}S_{\text{nano}}X_{\text{nano-eq}} + kSX_{\text{eq}})/(k_{\text{nano}}S_{\text{nano}} + kS)$. Note that eq D3 is an exponential function, and therefore, the absolute value of the gradient becomes smaller as time proceeds. Using this property, we can estimate the value of $|J_{\text{nano-dissol}} - J_{\text{format}}|$ at time t_1:

$$\begin{aligned}&|J_{\text{nano-dissol}}(t_1) - J_{\text{format}}(t_1)| \\ &= \left|\left(\frac{dX_{\text{sol}}}{dt}\right)_{t=t_1}\right| \le \left|\frac{X_{\text{sol}}(t_1) - X_{\text{sol}}(t_0)}{t_1 - t_0}\right| \le \frac{X_{\text{nano-eq}}}{t_1 - t_0}\end{aligned} \tag{D4}$$

Combining eqs D1 with eq D4, we obtain the relation

$$\Delta t \equiv t_1 - t_0 \le \frac{X_{\text{nano-eq}}}{D_{\text{close}}J_{\text{nano-dissol}}} \tag{D5}$$

Using eq D5, we can estimate the time needed for a small D_{close} value. For example, when pH is 6 and the temperature is 297 K,[2]

$$\begin{aligned}X_{\text{nano-eq}} &= 3.2 \times 10^{-5}\ [\text{mol L}^{-1}] \\ J_{\text{nano-dissol}} &= 1.67 \times 10^{-4}\ [\text{mol L}^{-1}\ \text{day}^{-1}]\end{aligned} \tag{D6}$$

Substituting eq D6 and $D_{\text{close}} = 0.01$ into eq D5, we obtain $\Delta t \le 0.19$ day. This is a very short time compared with the half-life time of ferrihydrite (166 days) at pH 6 and 297 K, indicating that J_{format} becomes almost equal to $J_{\text{nano-dissol}}$ quickly.

Appendix E

We here calculate the ratio of the active surface area of nanoparticles to that of crystals. The ratio is given by

$$\frac{S_{\text{nano}}(t)}{S(t)} = \frac{S_{\text{dead}}(\infty)}{S(t)}\frac{S_{\text{nano}}(t)}{S_{\text{dead}}(\infty)} \tag{E1}$$

where S_{dead} is the surface area of crystals that do not grow. The first term of the right side of eq E1 is converted to

$$\begin{aligned}\frac{S_{\text{dead}}(\infty)}{S(t)} &= \frac{\lim_{t\to\infty}\int_{t_{\text{inflec}}}^{t} 4\pi(r_{\max})^2 N(\tau) I\, d\tau}{\int_{t-t_{\text{inflec}}}^{t} 4\pi\{(t-\tau)G\}^2 N_{\text{nano}}(\tau) I\, d\tau} \\ &= \frac{(r_{\max})^2 \lim_{t\to\infty}\int_{0}^{t-t_{\text{inflec}}} N(\tau) I\, d\tau}{\int_{t-t_{\text{inflec}}}^{t}\{(t-\tau)G\}^2 N_{\text{nano}}(\tau) I\, d\tau}\end{aligned} \tag{E2}$$

Substituting $N_{\text{nano}}(\tau) = M_{\text{nano}}(0)R_{\text{nano}}(\tau)/m_{\text{nano}}$ into eq E2, we obtain

$$\frac{S_{\text{dead}}(\infty)}{S(t)} = \frac{(r_{\max})^2 \lim_{t\to\infty}\int_{t_{\text{inflec}}}^{t} R(\tau)\, d\tau}{\int_{t-t_{\text{inflec}}}^{t}\{(t-\tau)G\}^2 R_{\text{nano}}(\tau)\, d\tau} \tag{E3}$$

Table E1. Values of S_{nano}/S

	S_{nano} / S			
b	$p = 0.1$	$p = 0.2$	$p = 0.5$	$p = 1.0$
0.1	280	139	78.6	71.2
0.2	278	130	51.6	36.5
0.3	278	128	46.2	24.3
0.4	278	128	41.4	21.3
0.5	278	128	37.7	18.5
0.6	278	128	35.0	15.6
0.7	278	128	32.7	12.8
0.8	278	128	30.4	9.9
0.9	278	128	28.0	6.7

Converting parameters with $\tau = t_{\mathrm{inflec}}\beta$ and $t = t_{\mathrm{inflec}}b$, we obtain

$$\frac{S_{\mathrm{dead}}(\infty)}{S(t_{\mathrm{inflec}}b)} = \frac{\lim_{t\to\infty}\int_1^b R(t_{\mathrm{inflec}}\beta)\,\mathrm{d}\beta}{\int_{b-1}^{b}(b-\beta)^2 R(t_{\mathrm{inflec}}\beta)\,\mathrm{d}\beta} \tag{E4}$$

By approximating the equation with summation instead of integration, we obtain

$$\frac{S_{\mathrm{dead}}(\infty)}{S(t_{\mathrm{inflec}}b)} = \frac{\sum_{i=n+1}^{\infty} R(t_{\mathrm{inflec}}(i-0.5)/n)}{\sum_{i=m-n+1}^{m}(m/n-(i-0.5)/n)^2 R_{\mathrm{nano}}(t_{\mathrm{inflec}}(i-0.5)/n)} \tag{E5}$$

where $b = m/n$. The second term of eq E1 is

$$\frac{S_{\mathrm{nano}}(t)}{S_{\mathrm{dead}}(\infty)} = \frac{S_{\mathrm{nano}}(0)}{S_{\mathrm{dead}}(\infty)}R_{\mathrm{nano}}(t) = \frac{4\pi(r_{\mathrm{nano}})^2 N_{\mathrm{nano}}(0)}{4\pi(r_{\max})^2 N_{\mathrm{dead}}(\infty)}R_{\mathrm{nano}}(t)$$

$$= \frac{4\pi(r_{\mathrm{nano}})^2 \dfrac{M_{\mathrm{nano}}(0)v_{\mathrm{nano}}}{(4\pi/3)(r_{\mathrm{nano}})^3}}{4\pi(r_{\max})^2 \dfrac{M(\infty)v}{(4\pi/3)(r_{\max})^3}}R_{\mathrm{nano}}(t) = \frac{r_{\max}v_{\mathrm{nano}}}{r_{\mathrm{nano}}v}R_{\mathrm{nano}}(t) \tag{E6}$$

As a result, S_{nano}/S is given by

$$\frac{S_{\mathrm{nano}}(t)}{S(t)} = \frac{\sum_{i=1}^{\infty} R(t_{\mathrm{inflec}}(i-0.5)/n)}{\sum_{i=m-n+1}^{m}(m/n-(i-0.5)/n)^2 R_{\mathrm{nano}}(t_{\mathrm{inflec}}(i-0.5)/n)} \times\frac{r_{\max}}{r_{\mathrm{nano}}}\frac{v_{\mathrm{nano}}}{v}R_{\mathrm{nano}}(t) \tag{E7}$$

Assuming that the ratio of $r_{\max}$ (about 50−100 nm) to r_{nano} (about 5−10 nm) is 10 and the ratio of molar volumes (v_{nano}/v) is one and using eq E7, we obtain the values of S_{nano}/S as functions of p and R (Table E1).

References

(1) Fischer, W. R.; Schwertmann, U. The formation of hematite from amorphous iron(III)hydroxide. *Clays Clay Miner*. **1975**, *23*, 33–37.
(2) Schwertmann, U.; Murad, E. Effect of pH on the formation of goethite and hematite from ferrihydrite. *Clays Clay Miner*. **1983**, *31*, 277–284.
(3) Nagano, T.; Nakashima, S.; Nakayama, S.; Senoo, M. The use of color to quantify the effects of pH and temperature on the crystallization kinetics of goethite under highly alkaline conditions. *Clays Clay Miner*. **1994**, *42*, 226–234.
(4) Schwertmann, U.; Stanjek, H.; Becher, H.-H. Long-term *in vitro* transformation of 2-line ferrihydrite to goethite/hematite at 4, 10, 15 and 25°C. *Clay Miner*. **2004**, *39*, 433–438.
(5) Shaw, S.; Pepper, S. E.; Bryan, N. D.; Livens, F. R. The kinetics and mechanisms of goethite and hematite crystallization under alkaline conditions, and in the presence of phosphate. *Am. Mineral*. **2005**, *90*, 1852–1860.
(6) Burleson, D. J.; Penn, R. L. Two-step growth of goethite from ferrihydrite. *Langmuir* **2006**, *22*, 402–409.
(7) Yee, N.; Shaw, S.; Benning, L. G.; Nguyen, T. H. The rate of ferrihydrite transformation to goethite via the Fe(II) pathway. *Am. Mineral*. **2006**, *91*, 92–96.
(8) Pierce, M. L.; Moor, C. B. Adsorption of arsenite on amorphous iron hydroxide from dilute aqueous solution. *Environ. Sci. Technol*. **1980**, *14*, 214–216.
(9) Swedlund, P. J.; Wester, J. G. Cu and Zn ternary surface complex formation with SO_4 on ferrihydrite and schwertmannite. *Appl. Geochem*. **2001**, *16*, 503–511.
(10) Waychunas, G. A.; Fuller, C. C.; Davis, J. A. Surface complexation and precipitate geometry for aqueous Zn(II) sorption on ferrihydrite I: X-ray absorption extended fine structure spectroscopy analysis. *Geochim. Cosmochim. Acta* **2002**, *66*, 1119–1137.
(11) Logue, B. A.; Smith, R. W.; Westall, J. C. U(VI) adsorption on natural iron-coated sands: comparison of approaches for modeling adsorption on heterogeneous environmental materials. *Appl. Geochem*. **2004**, *19*, 1937–1951.
(12) Novikov, A. P.; Kalmykov, S. N.; Utsunomiya, S.; Ewing, R. C.; Horreard, F; Merkulov, A.; Clark, S. B.; Tkachev, V. V.; Myasoedov, B. F. Colloids transport of plutonium in the far-field of the Mayak Production Association, Russia. *Science* **2006**, *314*, 638–641.
(13) Oehler, J. H. Hydrothermal crystallization of silica gel. *Geol. Soc. Am. Bul*. **1976**, *87*, 1143–1152.
(14) Li, Q.; Creaser, D.; Sterte, J. The nucleation period for TPA-silicalite-1 crystallization determined by a two-stage varying-temperature synthesis. *Microporous Mesoporous Mater*. **1999**, *31*, 141–150.
(15) Li, Q.; Mihailova, B.; Creaser, D.; Sterte, J. The nucleation period for crystallization of colloidal TPA-silicalite-1 with varying silica source. *Microporous Mesoporous Mater*. **2000**, *40*, 53–62.
(16) Li, Q.; Mihailova, B.; Creaser, D.; Sterte, J. Aging effects on the nucleation and crystallization kinetics of colloidal TPA-silicalite-1. *Microporous Mesoporous Mater*. **2001**, *43*, 51–59.
(17) Davis, T. M.; Drews, T. O.; Ramanan, H.; He, C.; Dong, J.; Schnablegger, H.; Katsoulakis, M. A.; Kokkoli, E.; Mccormick, A. V.; Penn, R. L.; Tsapatsis, M. Mechanical principles of nanoparticle evolution to zeolite crystals. *Nat. Mater*. **2006**, *5*, 400–408.
(18) Gilbert, B.; Zhang, H.; Huang, F.; Finnegan, M. P.; Waychunas, G. A.; Banfield, J. F. Special phase transformation and crystal growth pathways observed in nanoparticles. *Geochem. Trans*. **2003**, *4*, 20–27.
(19) Finnegan, M. P.; Zhang, H.; Banfield, J. F. Phase stability and transformation in titania nanoparticles in aqueous solutions dominated by surface energy. *J. Phys. Chem. C* **2007**, *111*, 1962–1968.
(20) Denkewicz, J. R. P.; TenHuisen, K. S.; Adair, J. H. Hydrothermal crystallization kinetics of *m*-ZrO_2 and *t*-ZrO_2. *J. Mater. Res*. **1990**, *5*, 2698–2705.
(21) Babarao, R.; Hu, Z.; Jiang, J.; Chempath, S.; Sandler, S. I. Storage and separation of CO_2 and CH_4 in silicalite, C_{168} schwarzite, and IRMOF-1: a comparative study from Monte Carlo simulation. *Langmuir* **2007**, *23*, 659–666.
(22) Fujishima, A.; Rao, T. N.; Tryk, D. A. Titanium dioxide photocatalysis. *Photochem. Rev*. **2000**, *1*, 1–21.
(23) Garvie, R. C.; Hannink, R. H.; Pascoe, R. T. Ceramic steel? *Nature* **1975**, *258*, 703–704.
(24) Avrami, M. Kinetics of phase changes 1. General theory. *J. Chem. Phys*. **1939**, *7*, 1103–1112.
(25) Avrami, M. Kinetics of phase change 2. Transformation-time relation for random distribution of nuclei. *J. Chem. Phys*. **1940**, *8*, 212–224.
(26) Avrami, M. Granulation, phase change and microstructure: Kinetics of phase change 3. *J. Chem. Phys*. **1941**, *9*, 177–184.
(27) Zhang, H.; Banfield, J. F. New kinetic model for the nanocrystalline anatase-to-rutile transformation revealing rate dependence on number of particles. *Am. Mineral*. **1999**, *84*, 528–535.
(28) Lasaga, A. C. *Kinetic theory in the earth sciences*; Princeton University Press: Princeton, NJ, 1998; Chapter 6−7, pp 497−712.
(29) Malkin, A. I.; Chernov, A. A.; Alexeev, I. V. Growth of dipyramidal face of dislocation- free ADP crystals; free energy of steps. *J. Cryst. Growth* **1989**, *97*, 765–769.
(30) Cornell, R. M.; Posner, A. M.; Quirk, J. P. Crystal morphology and the dissolution of goethite. *J. Inorg. Nucl. Chem*. **1974**, *36*, 1937–1946.

(31) Naumov, G. B.; Ryzhenko, B. N.; Khodakovsky, I. L. *Handbook of thermodynamic data*; Natl. Tech. Inf. Service, Pb-226, 722/7GA, U. S. Dept. Commerce, **1974**.
(32) Lu, K.; Wang, J. T. Crystallization kinetics of Ni-P glass activation energies for nucleation and growth of nuclei. *J. Mater. Sci.* **1988**, *23*, 3001–3005.
(33) Lu, K.; Wang, J. T. Activation energies for crystal nucleation and growth in amorphous alloys. *Mater. Sci. Eng.* **1991**, *A113*, 500–503.
(34) Schwertmann, U. Inhibitory effect of soil organic matter on the crystallization of amorphous ferric hydroxide. *Nature* **1966**, *212*, 645–646.
(35) Cornell, R. M.; Giovanoli, R.; Schindler, P. W. Effect of silicate species on the transition of ferrihydrite into goethite and hematite in alkaline media. *Clays Clay Miner.* **1987**, *35*, 21–28.
(36) Cornell, R. M.; Giovanoli, R.; Schindler, P. W. Effect of silicate species on the transition of ferrihydrite into goethite and hematite in alkaline media. *Clays Clay Miner.* **1987**, *35*, 21–28.
(37) Paige, C. R.; Snodgrass, W. J.; Nicholson, R. V.; Scharer, J. M.; He, Q. H. The effect of phosphate on the transformation of ferrihydrite into crystalline products in alkaline media. *Water Air, Soil, Pollut.* **1997**, *97*, 397–412.
(38) Tichang, Sun; Paige, C. R.; Snodgrass, W. J. The effect of cadmium on the transformation of ferrihydrite into crystalline products at pH 8. *Water Air, Soil, Pollut.* **1996**, *91*, 307–325.